Sensors and Actuators B 230 (2016) 434–441

Contents lists available at ScienceDirect

Sensors and Actuators B: Chemical

journal homepage: www.elsevier.com/locate/snb

Phosphorescent oxygen sensors produced from polyolefin fibres by solvent-crazing method

Swagata Banerjee[a], Olga V. Arzhakova[b], Alla A. Dolgova[b], Dmitri B. Papkovsky[a,*]

[a] School of Biochemistry and Cell Biology, University College Cork, Cavanagh Pharmacy Building, Cork, Ireland
[b] Faculty of Chemistry, Lomonosov Moscow State University, Leninskie Gory, Moscow 119991, Russian Federation

ARTICLE INFO

Article history:
Received 30 October 2015
Received in revised form 9 February 2016
Accepted 15 February 2016
Available online 21 February 2016

Keywords:
Solid-state oxygen sensor
Phosphorescence quenching
Polyolefin fibre
Solvent crazing

ABSTRACT

Development of phosphorescent oxygen sensing materials based on commercially available semicrystalline polymer fibres (polyolefins, PP and PE) is described. The Pt-benzoporphyrin dye was incorporated into the nanoporous network of polyolefin fibres formed upon tensile drawing in the presence of physically active liquid environment via the mechanism of solvent crazing. Optimised fibre sensors showed optimal sensitivity to O_2, stable calibration in the range of 0–21 kPa O_2, reversible operation, linear temperature dependence and no significant cross-sensitivity towards humidity. The high surface area to volume ratio of the solvent-crazed polymer fibres enabled relatively bright phosphorescence intensity signals and fast response. Widefield and confocal microscopy combined with lifetime imaging were used to investigate the fine structure, dye distribution and heterogeneity of quenching by O_2 in the solvent-crazed dye-containing polymer fibres.

1. Introduction

Sensors for molecular oxygen (O_2) based on the quenching of photoluminescent dyes and materials have received increasing attention due to their potential applications in food and pharmaceutical packaging [1–5], biological research [6–8], industrial process control, environmental monitoring and other areas [1]. Solid-state sensors are constructed by incorporating an O_2-sensitive phosphorescent dye into a suitable polymeric matrix, and the response towards O_2 is detected through measurement of the intensity or lifetime signals which are quenched by O_2 [1]. Unlike oxygen electrodes [9], they lack oxygen consumption, are able to monitor O_2 levels in a non-invasive, contact-less manner, and provide accurate quantification of O_2 in gas and liquid phases, fast and reversible response and excellent sensitivity in the low O_2 range [1,2].

Polymeric matrices, such as polystyrene (PS), polysulfone (Psu), silicones, ormosils exhibiting moderate to high O_2 permeability, high chemical and mechanical stability, are widely used to prepare oxygen sensors [1]. Sensor fabrication methods include casting of thin films on a suitable substrate using a cocktail of a dye and a polymer in an organic solvent [10], polymerization and curing of precursors (e.g., sol–gel, Ormosil) [11,12], covalent coupling of a dye to the polymer [13], incorporation of the dye into micro or nanoparticles, etc. [6,14]. The sensitivity and response dynamics of a sensor are dictated by the O_2 permeability, diffusion rate of O_2 through the polymer matrix, the lifetime of the dye and quenching efficiency.

Polyethylene (PE) and polypropylene (PP) based materials are widely used in packaging and as heat sealable layers [15]. These polymers exhibit moderate O_2 permeability, good chemical and mechanical stability, but their application in O_2 sensing has been limited by poor 'processability' and compatibility with established sensor fabrication technologies and dyes. Recently, solvent (or environmental) crazing of polymers has been suggested for the preparation of O_2 sensors from polymeric substrates, mainly films [16]. This method proved to be universal and allows production of O_2-sensitive materials from various semi-crystalline or glassy polymers. In solvent-crazing, a polymer substrate is subjected to tensile drawing in a physically active solvent at room temperature to a certain tensile strain. Two main modes of solvent crazing are known: the classical one for amorphous glassy polymers and delocalized solvent crazing for semicrystalline polymers [17]. During this procedure, porosity in semicrystalline polymers increases via interlamellar separation and fibrillation, forming a continuous nanoporous network with dimensions of pores and fibrils of ~10 nm [18]. If a phosphorescent O_2-sensitive dye (or other cargo) is dissolved in the crazing-assisting solvent, it gets physically

* Corresponding author.
E-mail address: d.papkovsky@ucc.ie (D.B. Papkovsky).

http://dx.doi.org/10.1016/j.snb.2016.02.062
0925-4005/

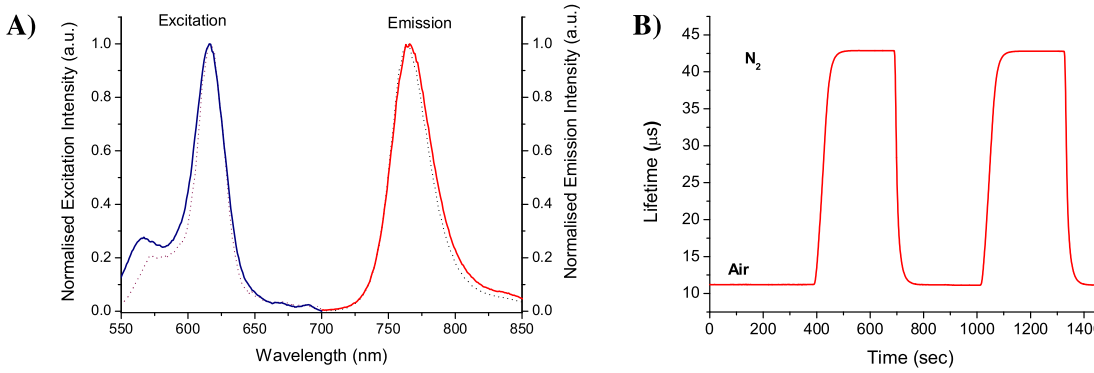

Fig. 1. (A) Excitation and emission spectra of PtBP in solvent-crazed SF3 fibre (solid line) and toluene (dotted line), λ_{ex} = 615 nm under N_2 atmosphere, (B) reversible response of SF3 at 20 °C.

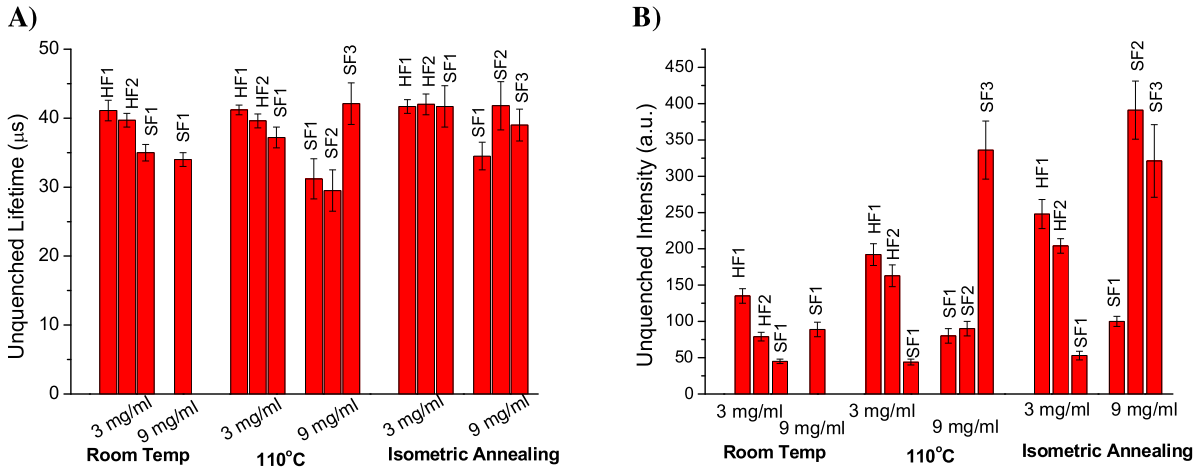

Fig. 2. The effect of post-crazing treatments on the unquenched (a) lifetimes and (b) intensities of various fibers dye concentrations of 3 mg/ml, and 9 mg/ml.

entrapped in the nanopores forming a phosphorescent O_2-sensitive material. This method was also adapted for the fabrication of discrete O_2 sensor spots from HDPE [19] and PPS films [20,21], coined as "spot or local" crazing. So far, most work on solvent-crazing was performed on commercial polymer films.

In recent years, micro- and nano-sized fibres have been explored with the view of production of sensors for various analytes [22–28]. Such materials display a number of special features (e.g. high sensitivity, fast response, high surface area to volume ratio, porosity, easy access to analytes), which also make them attractive for O_2 sensing applications. Nanofibres produced from polymers with moderate to high O_2 permeability including PS [27,29], biocompatible polymers such as polycaprolactone (PCL) [30] have been fabricated by solution-electrospinning method by applying an electric voltage to droplets of a homogeneous solution of the corresponding polymer in a suitable organic solvent [31,32]. The solution electrospinning method has also been applied to produce core-shell nanofibres using a poly(ether sulfone) (PES) or a polysulfone (PSU) core and polycaprolactone (PCL) shell [26], PDMS (core) and PCL (shell) [28]. The electrospun nanofibres possess very thin diameters (~several hundred nanometers) and display ultrafast response to oxygen, which is advantageous for their applications in biological field (such as monitoring cellular metabolism, tissue engineering, cancer cell research etc) [26,28]. However, large-scale production of nanofibres through this method requires use of large quantity of organic solvent, which can increase the production cost as well as can result in environmental pollution. Despite the wide range of application of solution based electrospinning method for a variety of polymers, use of this method for fabrication of polyolefin nanofibres at ambient temperature is relatively limited due to low solubility of polyolefins in common organic solvents and their high electrical resistivity [33,34]. Commonly, electrospun polyolefin nanofibres are produced from polymer melt [35,36]. However compared to solution based method, melt electrospinning technique requires additional heating setup and addition of additives and conductive materials to reduce the viscosity of polymer melt and increase the electrical conductance [35,37–39].

In this context, solvent crazing of polyolefin fibre polymers offers a convenient alternative for preparation of nanocomposite O_2-sensitive materials, involving relatively simpler set-up, less processing steps, lower production cost and compatible with large-scale production. Solvent crazing of fibre substrates was previously studied [40] for PET fibres (a typical glassy polymer) which showed that structural behavior of fibres upon solvent crazing appears to be appreciably different from that of films. Deformation of glassy polymers proceeds via classical crazing and is characterized by the formation of alternating crazes with their specific fibrillar-porous structure that can be loaded with dye, and the dye-free regions of dense bulk polymer. This structure of alternating dyed and undyed regions seems to be less advantageous for sensors as it produces non-uniform dye distribution in the polymer. Moreover, PET by itself is not a good material for O_2 sensors [8]. In contrast, semicrystalline polyolefins prove to be effective matrices for O_2 sensors. Deformation of semicrystalline polymers proceeds via delocalized crazing which, in contrast to classical crazing, provides uniform development of nanopores and porosity via interlamellar separation, thus ensuring uniform distribution of the dye within fibre [18]. To the best of our knowledge, no studies on solvent

crazing of semicrystalline fibres have been performed so far. We therefore decided to extend the use of solvent crazing method to semicrystalline polyolefin fibre for preparation of nanocomposite O_2-sensitive materials. This is the first attempt of solvent crazing of semicrystalline fibres. This approach is beneficial for the production of fibre-based sensors from cheap commercial fibres (PE and PP) and hollow fibers. These materials possess high surface area and contact area with analyte.

Here we describe several new types of O_2 sensors produced from commercial semicrystalline polyolefin microfibres (PE and PP) impregnated with a phosphorescent O_2-sensitive dye Pt(II)-benzoporphyrin (PtBP) by the solvent-crazing. The effects of basic process parameters such as conditions of solvent crazing (SC), porosity of the SC polymer samples, dye concentration, post-annealing of the SC samples on the final performance of the sensor were investigated. Sensor characterisation was performed by measuring the phosphorescence intensities and lifetime values at various O_2 and environmental conditions (temperature, humidity, gas/liquid phase). The dye distribution along the length and depth of the polymer fibre was investigated with widefield and confocal microscopy combined with phosphorescence lifetime imaging. These sensor materials and fabrication method involve a relatively simple set-up, and potentially allow the production of luminescent monofibres based on semicrystalline polymers in a cost-effective and scalable manner (continuous process).

2. Materials and methods

Hollow PP fibres, Type 1000 (HF1) and Type 3500 (HF2), thickness 40 μm were from Khimvolokno (Russia). Solid, 80 μm thick PP fibre (SF1) was from Textile Development Associates, USA. Solid, 40 μm thick PP fibre, Type 3500 (SF2) and PE fibre, Type 1000 (SF3) were from Khimvolokno (Russia). PtBP dye was from Luxcel Biosciences (Cork, Ireland); heptane – from Sigma–Aldrich; N_2 and O_2 gases (99.999% purity) – from Irish Oxygen (Ireland).

Impregnation of the polymer fibres was carried out by clamping and drawing a bundle of fibres in a custom-made drawing device [16] in *n*-heptane. PtBP dye was dissolved in *n*-heptane (3 mg/ml or 9 mg/ml), which was then used as crazing solvent for tensile drawing of the PP and PE fibres at a constant strain rate of 5 mm/min at room temperature. The solid fibres were stretched by 100% and hollow fibres—by 150%. After stretching fibres were released either at room temperature or at elevated temperature. Alternatively, the stretched fibres were annealed under isometric conditions at 110 °C for 30 min resulting in solvent-crazed fibres with open porosity. To enhance the development of crazing, SF1 was pre-annealed at 110 °C for 30 min prior to stretching.

3. Spectroscopic characterisation of the sensors

Phosphorescence measurements were carried out on a Cary Eclipse fluorescence spectrometer (Varian) equipped with a Peltier temperature control, with λ_{ex} = 620 nm, total decay time 0.02 sec, delay time 0.1 ms, gate time 5 ms. Excitation spectra were recorded using λ_{em} = 765 nm under similar set-up.

Initial screening was performed by fixing small bundles of the solvent-crazed fibres on a white paper background and measuring the phosphorescence intensity and lifetime values with a Firesting™ instrument (PyroSciences GmbH, Germany) equipped with a 1 mm fibre-optic probe and operated under standard manufacturer's settings (100% LED), at 20 °C in a flow cell. Phase shift values obtained from the Firesting™ instrument was converted into lifetimes using the equation: $\tau = \tan\theta/2\pi\vartheta$, where τ is the lifetime of the dye in seconds, θ is the phase shift (radian), and ϑ is the

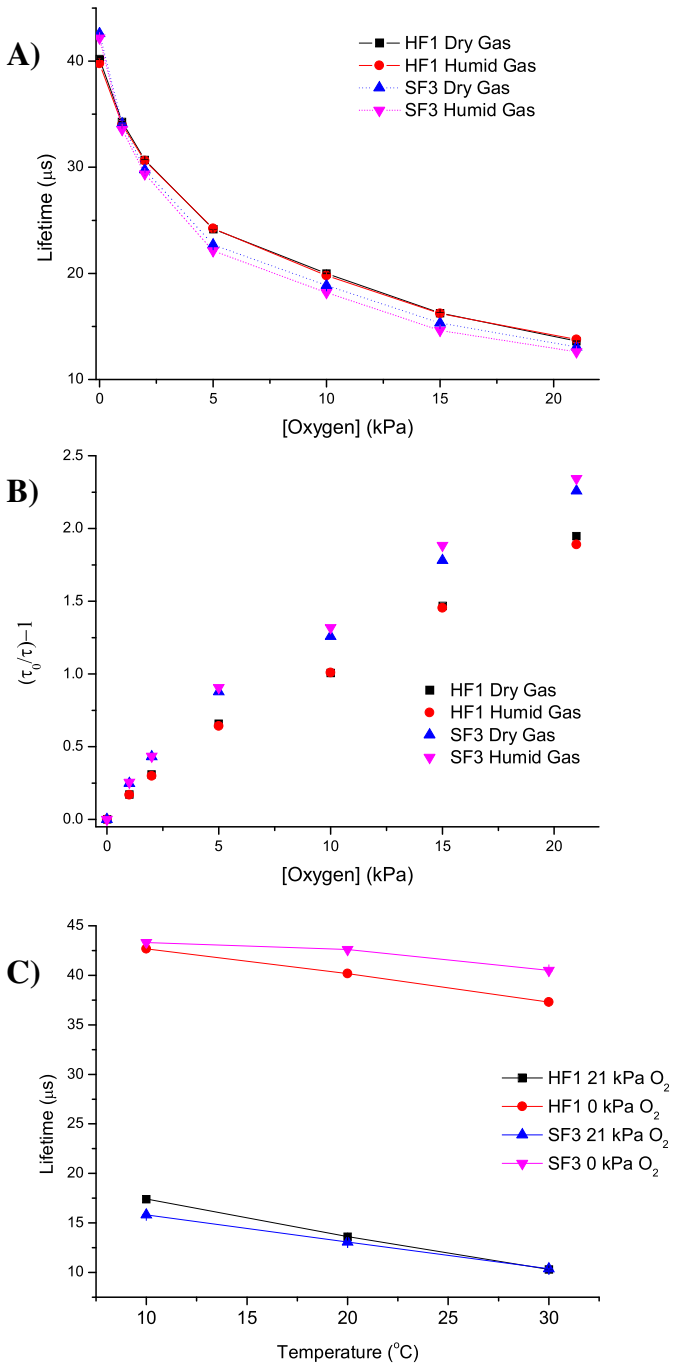

Fig. 3. (A) Dependence of phosphorescence lifetime on O_2 concentration for HF1 and SF3 in dry and humid gas mixtures at 20 °C; (B) corresponding Stern-Volmer plots, and (C) temperature dependence (in dry gas).

modulation frequency (4.0 kHz, which is close to optimal for the dye and range of lifetime changes or O2 concentrations studied).

Oxygen calibration was performed with the optimised sensor at 10, 20 and 30 °C. Standard O_2–N_2 gas mixtures (0–21 kPa O_2) produced using a precision gas mixer (LN Industries, Switzerland) were pumped through the flow-cell. The sensor was allowed to equilibrate for 10 min at each oxygen concentration and the signal was recorded with Firesting™. The reversibility of the sensors were examined by measuring phosphorescence signal by subjecting the sensors to alternate streams of N_2 and air. The response ($t_{90}\downarrow$) time was taken as the time required for the luminescence signal to decrease by 90% of the total change respectively.

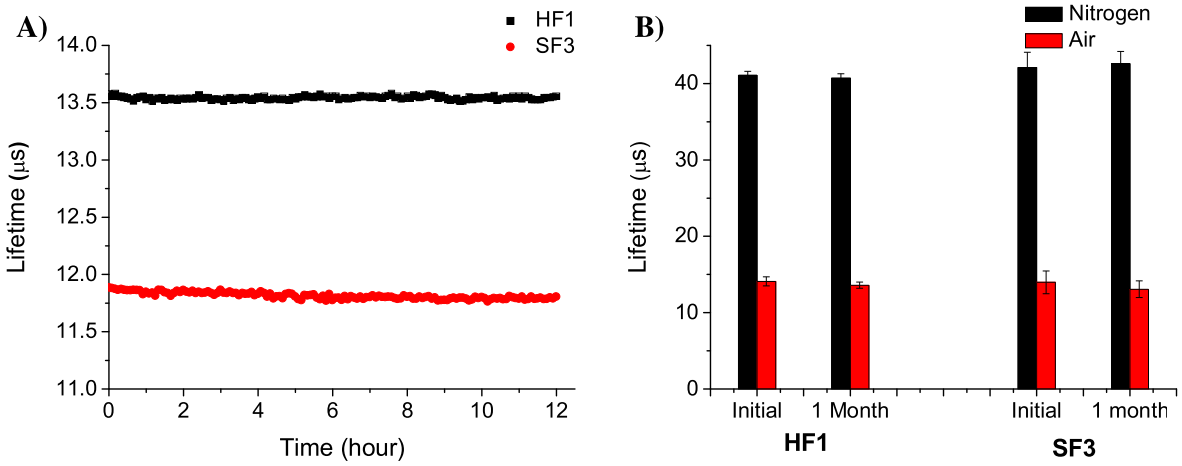

Fig. 4. (A) Photostability data for HF1 and SF3 upon continuous illumination for 12 h in air at 20 °C, (B) Lifetime data for HF1 and SF3 after one month storage at room temperature.

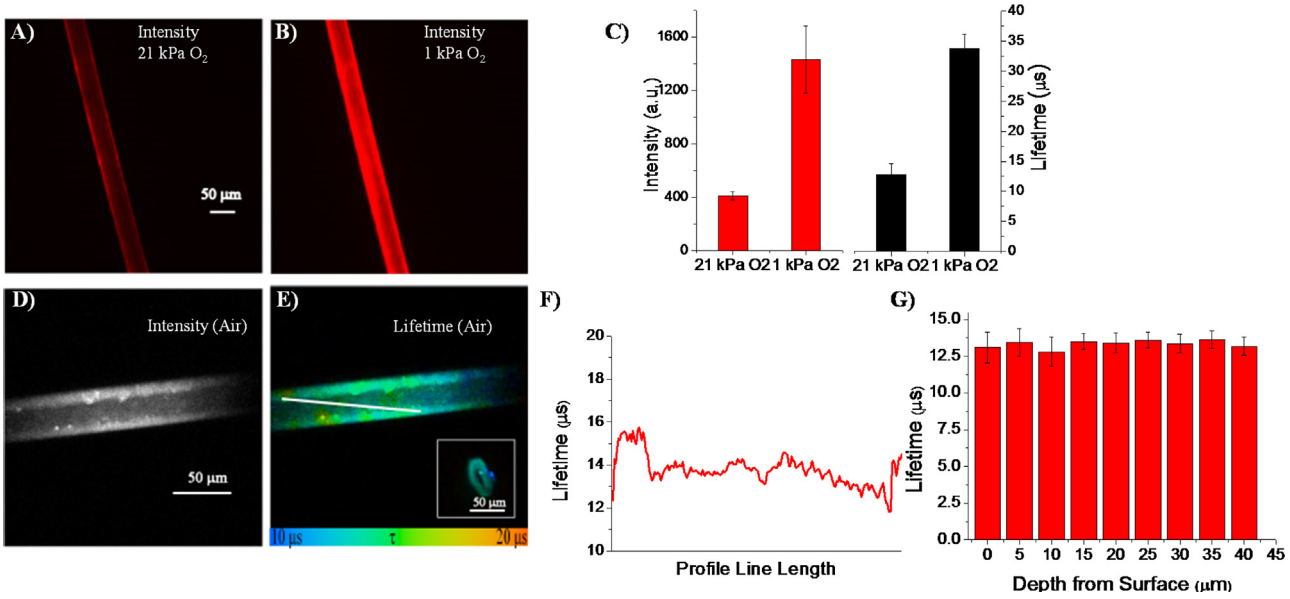

Fig. 5. Microscopic analysis of HF1 sensors: widefield intensity images at (A) 21 kPa and (B) 1 kPa O_2, (C) variation of intensity and lifetime values along the fibre length. (D) Confocal intensity and (E) lifetime images in air at 25 μm depth with Inset showing the edge of HF1. (F) and (G) show the variation of lifetime along the length and depth respectively.

4. Microscopic Characterisation

Widefield imaging was conducted on an inverted microscope Axiovert 200 (Carl Zeiss, Goettingen, Germany) equipped with a Plan Neofluar 10X/0.3 objective, pulsed excitation module (590 nm LED), gated CCD camera (LaVision Biotech), excitation (595/40 nm) and emission (780/60 nm) filter cubes and incubation chamber with O_2/CO_2/temperature control (Pecon) [41]. The differential interference contrast (DIC) and phosphorescence intensity images were obtained using exposure times 20 ms and 150 ms respectively. Phosphorescence lifetime imaging (PLIM) analysis was performed by collecting a set of frames (11) at different delay times, using pulse length 7 μs, exposure time 300 ms, 2 × 1 binning, and axis parameter 0–200 μs, for SF3 and exposure time 500 ms, axis parameter 0–150 μs (11 images) and 2 × 1 binning for HF1. The intensity signals of the frames were then fitted with single-exponential decay function to work out lifetime values for each pixel and produce 2D lifetime images of the sample.

Confocal microscopy and PLIM analysis were performed on a TCSPC-PLIM system (Becker & Hickl, Germany) based on an upright fluorescence microscope Axio Examiner Z1 (Zeiss) equipped with 40 × /1.1 W-LD-C Apochromat objective, temperature controlled stage, motorised *Z*-axis control, a DCS-120 confocal scanner (B&H), a R10467U-40 photon counting detector (Hamamatsu) connected to the scanner and controlled by TCSPC hardware [41]. The dye was excited at 614 nm with a tunable picosecond laser SC400-4 (Fianium, UK) and phosphorescence was collected with 750–810 nm band-pass and 665 nm long-pass filters. PLIM analysis was carried by fitting the decay traces with monoexponential decay functions using the built-in SPCImage software (B&H).

5. Results and discussion

5.1. Sensor fabrication and initial optimisation

Deformation of the fibres used in this study in the presence of a physically active solvent proceeds via the mechanism of delocalized

Table 1
Effect of various parameters on the lifetime and intensities of sensor fibres.

Post-crazing treatment	Dye conc.(mg/ml)	Fibre	LT (t) ms		t_0/t_{21}	Intensity a.u.		I_0/I_{21}
			21% O_2	0 % O_2		21% O_2	0 % O_2	
Shrinkage at room-temp. (Closed Pores)	3	HF1	12.5 ± 0.5	41.1 ± 1.5	3.3	54 ± 6	135 ± 10	2.5
		HF2	9.5 ± 0.8	39.7 ± 1.0	4.2	24 ± 2	79 ± 6	3.2
		SF1	6.0 ± 0.5	35.0 ± 1.2	5.8	14 ± 1	45 ± 3	3.2
	9	SF1	8.0 ± 1.0	34.0 ± 1.0	4.3	22 ± 2	89 ± 10	4.0
Shrinkage at 110 °C (Closed Pores)	3	HF1	14.8 ± 0.5	41.2 ± 0.7	2.8	90 ± 10	192 ± 15	2.1
		HF2	12.2 ± 0.5	39.61.0	3.2	61 ± 5	163 ± 15	2.7
		SF1	6.0 ± 0.5	37.2 ± 1.5	6.2	11 ± 1	44 ± 4	4.0
	9	SF1	15 ± 1.3	31.2 ± 2.9	2.1	44 ± 5	80 ± 10	1.8
		SF2	8.0 ± 1.0	29.5 ± 3.0	3.7	24 ± 3	90 ± 10	3.0
		SF3	11.0 ± 1.5	42.1 ± 3.0	3.8	117 ± 12	336 ± 40	2.9
Annealing under isometric conditions. (Open pores)	3	HF1	12.7 ± 0.7	41.7 ± 1.0	3.3	100 ± 15	248 ± 20	2.5
		HF2	12.7 ± 1.0	42.0 ± 1.5	3.3	68 ± 5	204 ± 10	3.8
		SF1	9.5 ± 1.0	41.7 ± 3.0	4.4	13 ± 1.5	53 ± 6	4.1
	9	SF1	12.8 ± 1.0	34.5 ± 2.0	2.7	34 ± 4	100 ± 7	2.9
		SF2	23.6 ± 2.5	39 ± 2.3	1.7	157 ± 20	321 ± 50	2.0
		SF3	23.0 ± 1.5	41.8 ± 3.5	1.8	172 ± 15	391 ± 40	2.3
Optimal Sensor HF1 (110 °C-shrinkage)			14.8 ± 0.5	41.2 ± 0.7	2.8	90 ± 10	192 ± 15	2.1
Optimal sensor SF3 (110 °C- shrinkage)			11.0 ± 1.5	42.1 ± 3.0	3.8	117 ± 12	336 ± 40	2.9

Table 2
Effect of humidity on the lifetime on sensor fibres.

Treatment		Dye conc(mg/ml)	Fibre	LT (t) ms Dry Gas		LT (t) ms Humud Gas	
				21% O2	0 % O_2	21% O_2	0 % O_2
Extension in dye containing solution	Shrinkage at room temp. (Closed Pores)	3	HF1	12.5 ± 0.5	41.1 ± 1.5	12.2 ± 0.4	41.5 ± 0.5
			HF2	9.5 ± 0.8	39.7 ± 1.0	9.3 ± 0.7	38.9 ± 1.0
			SF1	6.0 ± 0.5	35.0 ± 1.2	5.5 ± 0.5	35.0 ± 0.1
		9	SF1	8.0 ± 1.0	34.0 ± 1.0	7.9 ± 1.0	33.0 ± 1.0
	Shrinkage at 110°C (Closed Pores)	3	HF1	14.8 ± 0.5	41.2 ± 0.7	14.1 ± 0.5	40.9 ± 0.9
			HF2	12.2 ± 0.5	39.6 ± 1.0	12.0 ± 1.0	39.5 ± 0.8
			SF1	6.0 ± 0.5	37.2 ± 1.5	5.8 ± 0.5	36.8 ± 1.2
		9	SF1	15 ± 1.3	31.2 ± 2.9	14.2 ± 1.2	31.3 ± 2.6
			SF2	8.0 ± 1.0	29.5 ± 3.0	7.5 ± 1.0	29.0 ± 2.0
			SF3	11.0 ± 1.5	42.1 ± 3.0	10.5 ± 1.2	42.0 ± 2.0
	Annealing isometric cond. (Open pores)	3	HF1	12.7 ± 0.7	41.7 ± 1.0	12.5 ± 0.5	41.2 ± 0.5
			HF2	12.7 ± 1.0	42.0 ± 1.5	12.0 ± 0.6	42.7 ± 1.0
			SF1	9.5 ± 1.0	41.7 ± 3.0	8.0 ± 0.5	40.4 ± 0.6
		9	SF1	12.8 ± 1.0	34.5 ± 2.0	10.0 ± 1.0	32.0 ± 2.0
			SF2	23.6 ± 2.5	39 ± 2.3	21.0 ± 2.0	37.0 ± 2.0
			SF3	23.0 ± 1.5	41.8 ± 3.5	22.0 ± 1.5	40.0 ± 2.0

solvent crazing. Upon tensile drawing in the dye-containing solution, the fibres became brightly coloured in green, which directly indicates the development of open-pore structures in the polymer and proves incorporation of dye molecules into the nanopores. The porosity of fibers is shown to increase with increasing tensile strain. For our further studies the fibres with maximal (40%) porosity were selected: 100% for PE and PP fibers and 150% for hollow PP fibres. Pore sizes for the solvent-crazed fibers lie in the range 5–8 nm. Let us mention that the stretched fibers contain no visible crazes but appear to be uniformly colored along their length.

Fig. 1 illustrates the phosphorescence spectra of PtBP-doped SF3 fibre, with characteristic excitation Q-bands at 566 nm and 615 nm, and emission band centred at 765 nm. All other fibres showed similar spectral characteristics. Compared to toluene, PtBP did not exhibit any significant spectral shift, when incorporated in polyolefin fibres through solvent crazing. The solvent-crazed fibres showed fast and reversible response, when exposed to alternating streams of air and N_2 (Fig. 1B).

Following the spectral characterisation of the dye-doped fibres, sensor fabrication was optimised by varying fibre type, dye concentration, and post-crazing treatments. Initially HF1, HF2 and SF1 fibres were used, stretched in *n*-heptane containing 3 mg/ml PtBP. They were subsequently either released to their free state or annealed under isometric conditions at 110 °C. The effects of these treatments and impregnation on the phosphorescence lifetime and intensity signals of the fibres are summarised in Fig. 2A and B and Table 1. Dye concentrations below 3 mg/ml mainly reduced the intensity signals, which was undesirable.

All SC fibres annealed under isometric conditions showed higher unquenched lifetime and intensities (Fig. 2A and B). This probably results from the higher volume porosity of this material, thereby allowing higher dye incorporation, as well as redistribution of the dye molecules along the highly porous network of the SC-fibres and reduced dye aggregation after annealing [42]. However, the SC fibres annealed under isometric conditions showed high sensitivity to humidity (Table 2), which can be explained by their open porous structure. The fibres relaxed in free-standing state showed weaker signals, and this is perhaps correlated with reduced volume porosity [42] and thus lower dye loading. When the samples were allowed to shrink at 110 °C, their unquenched phosphorescence signal was higher than for the fibres relaxed at room temperature. This can be related to a more homogeneous distribution of dye molecules within the polymer network upon relaxation at elevated temperatures [19]. In all cases, SF1 displayed low unquenched intensities and lifetime values. Aiming to increase the intensity signals, we performed solvent crazing of SF1 in *n*-heptane containing 9 mg/ml PtBP, however, this decreased unquenched lifetime from 37.2 ± 1.5 μs to 33.0 ± 2.0 μs. This shortening of the lifetime can be explained by local overloading of the dye molecules resulting in their self-quenching and aggregation within the nanoporous

Table 3
Parameters of quenching by O_2 for HF1 and SF3.

Sensor	Temp (°C)	τ_0 (μs)	K^1_{SV} (kPa^{-1})	K^2_{SV} (kPa^{-1})	f	k^1_q(Pa^{-1}s^{-1})	k^2_q(Pa^{-1}s^{-1})
HF1	10	42.7	0.026	0.324	0.55	0.609	7.588
	20	40.8	0.037	0.390	0.51	0.907	9.559
	30	37.3	0.043	0.449	0.43	1.153	12.038
SF3	10	43.3	0.031	0.438	0.54	0.716	10.115
	20	42.6	0.037	0.533	0.47	0.869	12.512
	30	40.5	0.039	0.681	0.41	0.962	16.815

$k_q = K_{SV}/\tau_0$.

structure. The solvent-crazed SF2 and SF3 fibres after isometric annealing exhibited higher unquenched signals (Fig. 2A-B), but showed cross-sensitivity to humidity similar to SF1 (Table 2) and deemed less-suitable for O_2 sensing applications.

Among the fabricated sensors, solvent-crazed HF1 fibres prepared via tensile drawing at low dye concentration (3 mg/ml) with subsequent free-standing relaxation at 110 °C appeared to be the best performing ones. They exhibited higher unquenched lifetime and intensity signals and practically no cross-sensitivity with humidity (Table 2). Among solid fibres, SF3 prepared via stretching at high dye concentration and relaxation in free state at 110 °C was preferred over the other solid fibres. These samples were further studied in detail.

5.2. Detailed Characterisation

HF1 and SF3 sensor fibres were calibrated over 0–21 kPa O_2 at temperatures 10, 20 and 30 °C (Fig. 3A), and changes in phosphorescence lifetime were analysed by the Stern-Volmer plots (Fig. 3B). Both sensors showed non-linear behaviour at all the temperatures studied, which is indicative of heterogeneous micro-environments of the dye in the polymer. O_2 calibration data points were fitted with "Two Site model" which assumes two distinct quenching states of the dye [43,44]:

$$\frac{I}{I_0} = \frac{\tau}{\tau_0} = \frac{f}{1 + K^1_{SV}[O_2]} + \frac{(1-f)}{1 + K^2_{SV}[O_2]}$$

where I and τ represent the luminescence intensity and lifetime of the dye at any quencher concentration, I_0 and τ_0 represent the unquenched luminescence intensity and lifetime, f is the fraction of the total emission arising from first binding site, $K^1_{SV}$and K^2_{SV} correspond to the Stern–Volmer constants for two emitting components. From the fitting, model parameters (K^1_{SV}, K^2_{SV}, f) and calibration function were determined.

As expected, sensor fibres showed significant temperature dependence of quenching, which has to be compensated for. Table 3 shows that the unquenched lifetime signal for HF1 decreased from 42.7 μs at 10 °C to 37.3 μs at 30 °C (Fig. 3C), with a concomitant increase in the K_{SV} and bimolecular quenching constant k_q ($k_q = K_{SV}/\tau_0$). The average k_q values for the PE and PP fibres were significantly higher than for the corresponding planar sensors [19,45], indicative of their higher sensitivity to oxygen. The combination of high O_2 sensitivity and lack of cross-sensitivity towards humidity (Fig. 3A and Table 2) is advantageous for sensing of dissolved O_2.

Both HF1 and SF3 exhibited fully reversible response in dry and humid gas mixtures. In dry gas, HF1 and SF3 showed fast response with $t_{90}\downarrow$ values 60 s and 30 s, respectively. In humid gas mixture, $t_{90}\downarrow$ was 95 s for HF1 and 60 sec for SF3. For comparison, PP membranes exhibited slower response and recovery (~5 min) [45]. A general problem associated with luminescent sensors is degradation of the luminescent dye or sensor material upon continuous irradiation or long term storage. Photostability of the sensor fibres was investigated by measuring the phosphorescence signal in air at 20 °C. Upon continuous illumination over 12 h, no significant reduction in lifetime signals was observed (Fig. 4A). The sensor fibres also showed reproducible lifetime values over a period of one month (Fig. 4B), when stored in dark condition at room temperature. Their stability over further longer period of time is under investigation.

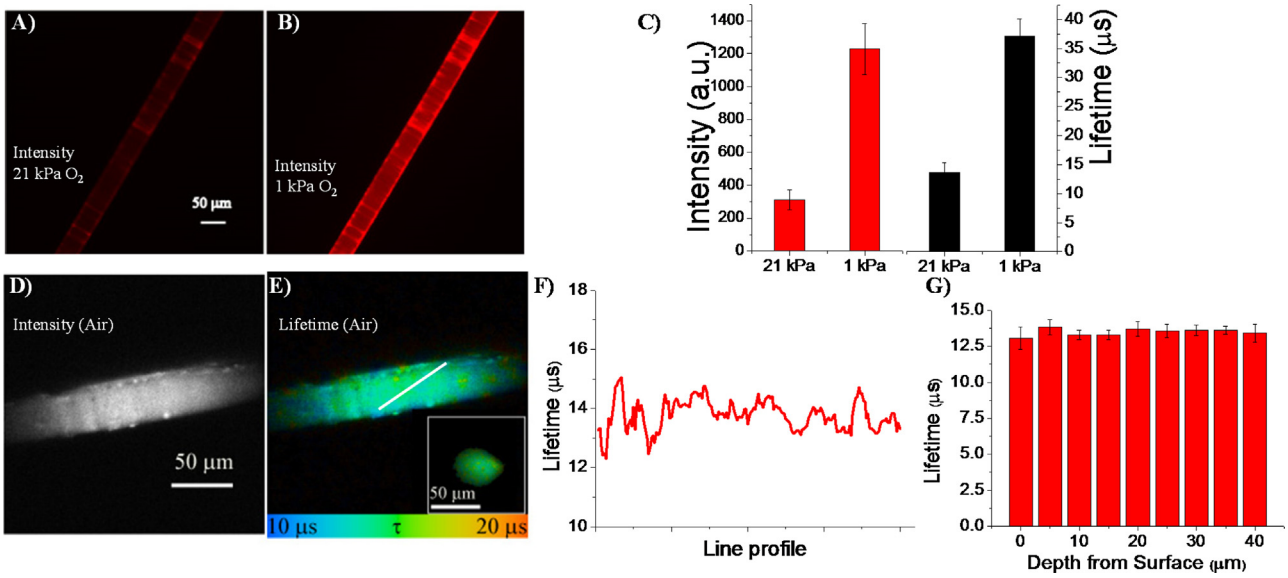

Fig. 6. Microscopic analysis of SF3 sensors: widefield intensity images at (A) 21 kPa and (B) 1 kPa O_2, 9 (C) variation of intensity and lifetime along the fibre length. (D) Confocal intensity and (E) lifetime images in air at 25 μm depth with Inset showing the edge of SF3, (F) and (G) demonstrate the variation of lifetime along the length and depth respectively.

Wide-field fluorescence microscopy combined with phosphorescence lifetime imaging (PLIM) were used to study the impregnation of the polymer fibres and lifetime signals at 21 kPa and 1 kPa O_2 concentrations (Fig. 5 and 6). A relatively uniform dye distribution (intensity) and a narrow lifetime distribution was observed along the HF1 fibre (Fig. 5A,B,C). The variability of lifetimes (12.8 ± 1.5 μs at 21 kPa and 33.7 ± 2.5 μs at 1 kPa of O_2) in PLIM was however, greater than for macroscopic measurements using Firesting™.

In the case of SF3, alternating band regions with higher intensities can be seen along the length of the fibres, consistent with the presence of alternating regions of nanoporous crazes in bulk polymers (Fig. 6A,B). Lifetimes at 21 kPa and 1 kPa showed narrow distribution: 13.6 ± 1.5 μs at 21 kPa O_2 and 37.1 ± 3.0 μs at 1 kPa O_2 (Fig. 6C).

The 3D structure and homogeneity of HF1 and SF3 sensor fibres were also studied by confocal PLIM microscopy. Their intensity and lifetime images at 25 μm depth from the surface are shown in Fig. 5 and 6D,E respectively. HF1 exhibited more uniform dye distribution across fibre. The hollow part of HF1 fibre showed reduced intensity signals. The lifetime distribution across the diameter of HF1 shown in Fig. 5E-inset demonstrated a uniform dye distribution with very few aggregates present on the surface with slightly lower lifetime. SF3 exhibited a heterogeneous distribution along the fibre length (Fig. 6F), although the lifetime did not vary significantly across the depth (Fig. 6G). The heterogeneous lifetime distribution along fibre length is probably due to localisation of dye into alternating crazes and bulk polymer phases formed during the solvent-crazing process.

6. Conclusion

For the first time, O_2 sensors based on semicrystalline polyolefin fibres were prepared by the incorporation of phosphorescent PtBP dye into polymer via the mechanism of delocalized solvent crazing. Among the sensors studied, the PP-based HF1 sensor appeared to be the best performing one. The sensors showed stable calibration in the range of 0–21 kPa O_2, linear temperature dependence and no significant cross-sensitivity towards humidity and uniform dye distribution. The high surface area to volume ratios of the fibres allows optimal sensitivity to O_2, rapid and reversible response. Sensor fabrication is simple, low-cost and compatible with large-scale industrial production in continuous mode. These fibre materials can find use as microsensor tips or on micromanipulator for probing O_2 levels in small samples and various applications including biological, medical and industrial. The polyolefin fibres offer advantages of being flexible, stable and robust. They can be used to produce new woven materials and smart textiles.

Ackowledgements

Financial support of this work by the Irish Department of Agriculture, Food and Marine, grant DAFM 11/F/015 and by Russian Foundation for Basic Research (RFBR), research project no. 14-03-00617a, is gratefully acknowledged. The authors wish to thank Dr R. Dmitriev, Dr I. Okkelman and Mr J. Jenkins for the help during the imaging experiments.

References

[1] X.-D. Wang, O.S. Wolfbeis, Optical methods for sensing and imaging oxygen: materials, spectroscopies and applications, Chem. Soc. Rev. 43 (2014) 3666–3761.
[2] O.S. Wolfbeis, Luminescent sensing and imaging of oxygen: fierce competition to the Clark electrode, Bioessays 37 (2015) 921–928.
[3] M. Quaranta, S. Borisov, I. Klimant, Indicators for optical oxygen sensors, Bioanal. Rev. 4 (2012) 115–157.
[4] X. Meng, S. Kim, P. Puligundla, S. Ko, Carbon dioxide and oxygen gas sensors-possible application for monitoring quality, freshness, and safety of agricultural and food products with emphasis on importance of analytical signals and their transformation, J. Korean Soc. Appl. Biol. Chem. 57 (2014) 723–733.
[5] A. Hempel, M.G. O'Sullivan, D.B. Papkovsky, J.P. Kerry, Nondestructive and continuous monitoring of oxygen levels in modified atmosphere packaged ready-to-eat mixed salad products using optical oxygen sensors, and its effects on sensory and microbiological counts during storage, J. Food Sci. 78 (2013) S1057–S1062.
[6] R.I. Dmitriev, S.M. Borisov, H. Duessmann, S. Sun, B.J. Mueller, J. Prehn, et al., versatile conjugated polymer nanoparticles for high-resolution O_2 imaging in cells and 3D tissue models, Acs Nano 9 (2015) 5275–5288.
[7] J. Jenkins, R.I. Dmitriev, K. Morten, K.W. McDermott, D.B. Papkovsky, Oxygen-sensing scaffolds for 3-dimensional cell and tissue culture, Acta Biomater. 16 (2015) 126–135.
[8] D.B. Papkovsky, R.I. Dmitriev, Biological detection by optical oxygen sensing, Chem. Soc. Rev. 42 (2013) 8700–8732.
[9] L.C. Clark, R. Wolf, D. Granger, Z. Taylor, Continuous recording of blood oxygen tensions by polarography, J. Appl. Physiol. 6 (1953) 189–193.
[10] S. Banerjee, R.T. Kuznetsova, D.B. Papkovsky, Solid-state oxygen sensors based on phosphorescent diiodo-borondipyrromethene dye, Sens. Actuators B 212 (2015) 229–234.
[11] C.-S. Chu, C.-Y. Chuang, Ratiometric optical fiber dissolved oxygen sensor based on metalloporphyrin and CdSe quantum dots embedded in sol–gel matrix, J. Lumin. 167 (2015) 114–119.
[12] I. Klimant, F. Ruckruh, G. Liebsch, C. Stangelmayer, O.S. Wolfbeis, Fast response oxygen micro-optodes based on novel soluble ormosil glasses, Mikrochim. Acta 131 (1999) 35–46.
[13] B.J. Müller, T. Burger, S.M. Borisov, I. Klimant, High performance optical trace oxygen sensors based on NIR-emitting benzoporphyrins covalently coupled to silicone matrixes, Sens. Actuators B 216 (2015) 527–534.
[14] B. Korzeniowska, M. Raspe, D. Wencel, R. Woolley, K. Jalink, C. McDonagh, Development of organically modified silica nanoparticles for monitoring the intracellular level of oxygen using a frequency-domain FLIM platform, RSC Adv. 5 (2015) 36938–36947.
[15] in: S. Ebnesajjad Plastic Films in Food Packaging, William Andrew Publishing Oxford 2013.
[16] R.N. Gillanders, O.V. Arzhakova, A. Hempel, A. Dolgova, J.P. Kerry, L.M. Yarysheva, et al., Phosphorescent oxygen sensors based on nanostructured polyolefin substrates, Anal. Chem. 82 (2009) 466–468.
[17] Front Matter, in: A.L. Volynskii, N.F. Bakeev (Eds.), Studies in Polymer Science, Elsevier, 1995, p. iii.
[18] A.L. Volynskii, N.F. Bakeev, A new approach to the preparation of nanocomposites based on a polymer matrix, Polym. Sci. Ser. C 53 (2011) 35–47.
[19] C. Toncelli, O.V. Arzhakova, A. Dolgova, A.L. Volynskii, N.F. Bakeev, J.P. Kerry, et al., Oxygen-sensitive phosphorescent nanomaterials produced from high-density polyethylene films by local solvent-crazing, Anal. Chem. 86 (2014) 1917–1923.
[20] C. Toncelli, O.V. Arzhakova, A. Dolgova, A.L. Volynskii, J.P. Kerry, D.B. Papkovsky, Phosphorescent oxygen sensors produced by spot-crazing of polyphenylenesulfide films, J. Mater. Chem. C 2 (2014) 8035–8041.
[21] C.A. Kelly, C. Toncelli, M. Cruz-Romero, O.V. Arzhakova, J.P. Kerry, D.B. Papkovsky, Phosphorescent O_2 sensors integrated in polymeric film materials by local solvent crazing, Mater. Des. 77 (2015) 110–113.
[22] X. Wang, C. Drew, S.-H. Lee, K.J. Senecal, J. Kumar, L.A. Samuelson, Electrospun nanofibrous membranes for highly sensitive optical sensors, Nano Lett. 2 (2002) 1273–1275.
[23] Y. Wang, B. Li, Y. Liu, L. Zhang, Q. Zuo, L. Shi, et al., Highly sensitive oxygen sensors based on Cu(i) complex-polystyrene composite nanofibrous membranes prepared by electrospinning, Chem. Commun. (2009) 5868–5870.
[24] Y. Yang, H. Wang, K. Su, Y. Long, Z. Peng, N. Li, et al., A facile and sensitive fluorescent sensor using electrospun nanofibrous film for nitroaromatic explosive detection, J. Mater. Chem. 21 (2011) 11895–11900.
[25] J. Yoon, S.K. Chae, J.-M. Kim, Colorimetric sensors for volatile organic compounds (VOCs) based on conjugated polymer-embedded electrospun fibers, J. Am. Chem. Soc. 129 (2007) 3038–3039.
[26] R. Xue, C. Ge, K. Richardson, A. Palmer, M. Viapiano, J.J. Lannutti, Microscale sensing of oxygen via encapsulated porphyrin nanofibers: effect of indicator and polymer core permeability, ACS Appl. Mater. Interfaces 7 (2015) 8606–8614.
[27] C. Wolf, M. Tscherner, S. Köstler, Ultra-fast opto-chemical sensors by using electrospun nanofibers as sensing layers, Sens. Actuators B 209 (2015) 1064–1069.
[28] R. Xue, P. Behera, J. Xu, M.S. Viapiano, J.J. Lannutti, Polydimethylsiloxane core? polycaprolactone shell nanofibers as biocompatible, real-time oxygen sensors, Sens. Actuators B 192 (2014) 697–707.
[29] L.-Y. Wang, Y. Xu, Z. Lin, N. Zhao, Y. Xu, Electrospinning fabrication and oxygen sensing properties of Cu(I) complex–polystyrene composite microfibrous membranes, J. Lumin. 131 (2011) 1277–1282.
[30] S.Y. Zhao, B.S. Harrison, Morphology impact on oxygen sensing ability of $Ru(dpp)_3Cl_2$ containing biocompatible polymers, Mater. Sci. Eng. C 53 (2015) 280–285.
[31] S. Ramakrishna, K. Fujihara, W.-E. Teo, T. Yong, Z. Ma, R. Ramaseshan, Electrospun nanofibers: solving global issues, Mater. Today 9 (2006) 40–50.

[32] B. Ding, M. Wang, X. Wang, J. Yu, G. Sun, Electrospun nanomaterials for ultrasensitive sensors, Mater. Today 13 (2010) 16–27.
[33] S.R. Givens, K.H. Gardner, J.F. Rabolt, D.B. Chase, High-Temperature electrospinning of polyethylene microfibers from solution, Macromolecules 40 (2007) 608–610.
[34] D.M. Rein, L. Shavit-Hadar, R.L. Khalfin, Y. Cohen, K. Shuster, E. Zussman, Electrospinning of ultrahigh-molecular-weight polyethylene nanofibers, J. Polym. Sci. Polym. Phys. 45 (2007) 766–773.
[35] R. Nayak, I.L. Kyratzis, Y.B. Truong, R. Padhye, L. Arnold, Melt-electrospinning of polypropylene with conductive additives, J. Mater. Sci. 47 (2012) 6387–6396.
[36] H. Li, W. Wu, M.M. Bubakir, H. Chen, X. Zhong, Z. Liu, et al., Polypropylene fibers fabricated via a needleless melt-electrospinning device for marine oil-spill cleanup, J. Appl. Polym. Sci. 131 (2014).
[37] A. Gora, R. Sahay, V. Thavasi, S. Ramakrishna, Melt-electrospun fibers for advances in biomedical engineering, clean energy, filtration, and separation, Polym. Rev. 51 (2011) 265–287.
[38] H. Zhou, T.B. Green, Y.L. Joo, The thermal effects on electrospinning of polylactic acid melts, Polymer 47 (2006) 7497–7505.
[39] L. Mascia, M. Xanthos, An overview of additives and modifiers for polymer blends: facts, deductions, and uncertainties, Adv. Polym. Tech. 11 (1992) 237–248.
[40] O.V. Arzhakova, A.A. Dolgova, L.M. Yarysheva, A.L. Volynskii, N.F. Bakeev, Specific features of the environmental crazing of poly(ethylene terephthalate) fibers, Polymer 56 (2015) 256–262.
[41] R.I. Dmitriev, A.V. Zhdanov, Y.M. Nolan, D.B. Papkovsky, Imaging of neurosphere oxygenation with phosphorescent probes, Biomaterials 34 (2013) 9307–9317.
[42] A.V. Volkov, M.A. Moskvina, A.A. Tunyan, A.I. Dement'ev, N.G. Yaryshev, A.L. Volynskii, et al., Specific features of the formation of polymer-dye systems based on nanostructured polymer matrices prepared by solvent crazing, Polym. Sci. Ser. A 52 (2010) 537–548.
[43] E.R. Carraway, J.N. Demas, B.A. DeGraff, J.R. Bacon, Photophysics and photochemistry of oxygen sensors based on luminescent transition-metal complexes, Anal. Chem. 63 (1991) 337–342.
[44] J.N. Demas, B.A. DeGraff, W. Xu, Modeling of luminescence quenching-based sensors: comparison of multisite and nonlinear gas solubility models, Anal. Chem. 67 (1995) 1377–1380.
[45] C.A. Kelly, C. Toncelli, J.P. Kerry, D.B. Papkovsky, Phosphorescent O_2 sensors based on polyolefin fabric materials, J. Mater. Chem. C 2 (2014) 2169–2174.

Biographies

Swagata Banerjee obtained her PhD (Chemistry) in 2013 from Trinity College Dublin, Ireland where her project focused on the synthesis and photophysical studies of fluorescent 1,8-naphthalimide derived DNA binders. After completing PhD, she joined CREST, Dublin Institute of Technology, where her research involved developing titania based functional materials and photocatalysis. She is currently working as a postdoctoral fellow in School of Biochemistry, University College Cork. Her research interest includes development of luminescent probes and materials for sensing and imaging applications.

Olga V. Arzhakova graduated from the Faculty of Chemistry, Lomonosov Moscow State University in 1982 and received her PhD in Chemistry in 1986. In 1991 she started her work as the scientific researcher at the Department of Polymers, Faculty of Chemistry, Lomonosov Moscow State University where she is now Associate Professor and Senior Researcher. Research interests of Dr.Arzhakova include physics and mechanics of solid polymers, crazing of polymers, nanoporous polymer materials, nanocomposite polymer-based materials, sensors and their applications, nanocatalysis, functional polymers, membranes.

Alla A. Dolgova graduated from the Faculty of Chemistry, Lomonosov Moscow State University in 1987 and received her PhD in Chemistry in 1994. In 1991 she started her work as the scientific researcher at the Department of Polymers, Faculty of Chemistry, Lomonosov Moscow State University where she is now Senior Researcher. Research interests of Dr. Dolgova include mechanical properties of solid polymers, crazing of polymers, nanoporous and nanocomposite polymer-based materials, sensors and their application, nanocatalysis, functional polymers.

Dmitri B. Papkovsky graduated from the Chemistry Department of Moscow State University in 1982 and received his PhD in 1986 from the Institute of Biochemistry, Russian Academy of Science, Moscow. In 1997 he joined Biochemistry Department of University College Cork, where he is currently Professor of Biochemistry and Head of Biophysics and Bioanalysis Lab. Research interests of Prof. Papkovsky include quenched-luminescence oxygen sensing and its applications, time-resolved and phase-resolved fluorescence spectroscopy, phosphorescence based probes and (bio) analytical techniques.